INSTITUTE OF PHYSICS PUBLISHING and INTERNATIONAL ATOMIC ENERGY AGENCY NUCLEAR FUSION

Nucl. Fusion **46** (2006) 921–927 doi:10.1088/0029-5515/46/11/006

Integrated physics optimization of a quasi-isodynamic stellarator with poloidally closed contours of the magnetic field strength

A.A. Subbotin[1], M.I. Mikhailov[1], V.D. Shafranov[1], M.Yu. Isaev[1], C. Nührenberg[2], J. Nührenberg[2], R. Zille[2], V.V. Nemov[3], S.V. Kasilov[3], V.N. Kalyuzhnyj[3] and W.A. Cooper[4]

[1] Russian Research Centre 'Kurchatov Institute', Moscow, Russia
[2] Max-Plank-Institut für Plasmaphysik, IPP-EURATOM Association, Germany
[3] Institute of Plasma Physics, National Science Center, 'Kharkov Institute of Physics and Technology', Kharkov, Ukraine
[4] Centre de Recherches en Physique des Plasmas, Association Euratom-Confédération Suisse, Ecole Polytechnique Fédérale de Lausanne, Switzerland

Received 23 February 2006, accepted for publication 6 September 2006
Published 28 September 2006
Online at stacks.iop.org/NF/46/921

Abstract
A quasi-isodynamic stellarator with poloidally closed contours of the magnetic field strength B (Mikhailov 2002 *Nucl. Fusion* **42** L23) has been obtained by an integrated physics optimization comprising MHD and neoclassical theory. For a configuration with six periods and aspect ratio approximately 12, a main result is the attainability of an essentially MHD-stable high-β ($\langle\beta\rangle \approx 0.085$) plasma with low neoclassical transport, approximately vanishing bootstrap current in the long-mean-free-path regime and excellent α-particle confinement.

PACS numbers: 52.20.Dq, 52.25.Xz, 52.30.Cv, 52.35.Py, 52.55.−s, 52.55.Hc

1. Introduction

In non-optimized stellarators the collisionless confinement times of energetic reflected particles are much shorter than their slowing-down time in a fusion-grade device. The achievement of such long collisionless confinement times in stellarators with a truly 3D structure of the field strength B is a computationally demanding problem if transitional particles (these are particles which are neither passing nor permanently reflected within one period) exist because they tend to get lost by collisionless stochastic diffusion [1]. A quasi-isodynamic (qi) stellarator with poloidally closed contours of B eliminates this class of particles and can exhibit excellent fast-particle confinement [2, 3]. Configurations of this type have sometimes been called quasi-poloidally symmetric. In contrast to quasihelical (qh) and quasi-axial (qa) symmetry, quasi-poloidal symmetry does not exist in any approximation in a toroidal plasma; therefore, here, the notion qi is preferred.

In this work, integrated stellarator optimization is used to show that high MHD-stable plasma β, low neoclassical transport, vanishing bootstrap (bs) current and good α-particle confinement can be achieved simultaneously for qi stellarators with poloidally closed contours of B.

2. Physics goals of the optimization

The conceptual core of the optimization is the strive for constancy of the second adiabatic invariant $\mathcal{J}$ on flux surfaces for all reflected particles in a configuration with poloidally closed contours of B [3]. Therefore, the latter property of a configuration is a prerequisite for this type of optimization. Earlier examples of qi optimization (see, e.g. [4]) were obtained by direct optimization of collisionless fast-particle confinement and did not have this property, but exhibited the strongest poloidal variation of B in the toroidal neighbourhood of their maximal magnetic field strength. On the other hand configurations exist in which the contours of B are poloidally closed in the region of maximal magnetic field strength because this just requires a straight plasma section in the neighbourhood of this maximum. In the integrated case study which will be discussed here, this property is approximately, but sufficiently, realized. An even closer approximation can easily be obtained

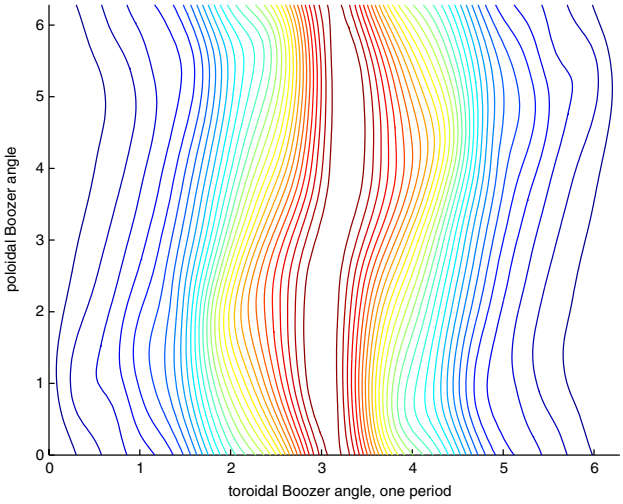

Figure 1. The contours of B on the magnetic surface (at half of the minor plasma radius) blue to red: minimum to maximum of B. It is seen that a very small residual local maximum of B still exists. The maximum is 1.55 while the first adjacent poloidally closed contour has $B = 1.51$, but is not shown in this figure for clarity.

by further optimization towards this property, as is seen in figure 1 by comparison with figure 3.

Ideal achievement of constancy of $\mathcal{J}$ on flux surfaces for all reflected particles in a configuration with poloidally closed contours of B has significant consequences for the ideal-MHD equilibrium as well as for the bootstrap current density: an ideal-MHD equilibrium without net toroidal current on a magnetic surface then has current density lines which close within one period and the bs current density then vanishes in the long-mean-free-path (lmfp) regime consistent with the assumption of vanishing net toroidal current. These statements are proven in the appendix.

In an integrated optimization, the coincidence of the $\mathcal{J}$ contours with the flux surfaces is not perfect so that other neoclassical properties have to be considered in addition. Besides the $\mathcal{J}$ contours, here the neoclassical equivalent ripple (characterizing the $1/\nu$ transport of the electrons) and the structural factor characterizing the bs current in the lmfp regime are evaluated by integration along field lines [5–7] and integrated into the penalty function of the optimization.

Further, as far as ideal MHD is concerned, besides evaluating the Mercier and resistive-interchange criteria [8], here the instability of possibly asymmetric (with respect to the stellarator symmetry of the configurations considered here) local ballooning modes [9] has now been integrated in the optimization.

Thus, the penalty function contains the deviation of the $\mathcal{J}$ contours from the magnetic surfaces, the neoclassical ripple and structural factor of the bs current, the Mercier and resistive-interchange criteria and asymmetric local ballooning modes. The independent variables of the optimization are the shape parameters of the plasma-boundary surface. Each evaluation of the penalty function requires a fixed-boundary VMEC [10] equilibrium as input for the evaluation of the above physics properties. The optimization in the space of boundary variables is unconstrained and performed with the NAG library (E04UCF).

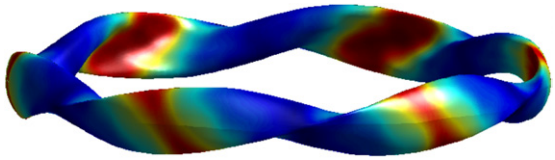

Figure 2. Boundary magnetic surface of the optimized configuration also showing the magnetic topography. The colours define the range of the magnetic field strength (red—maximum, blue—minimum, $(B_{\max} - B_{\min})/B \approx 0.5$). The characteristic feature of the configuration is the nearly vanishing curvature of the plasma column in the regions of the extrema of B.

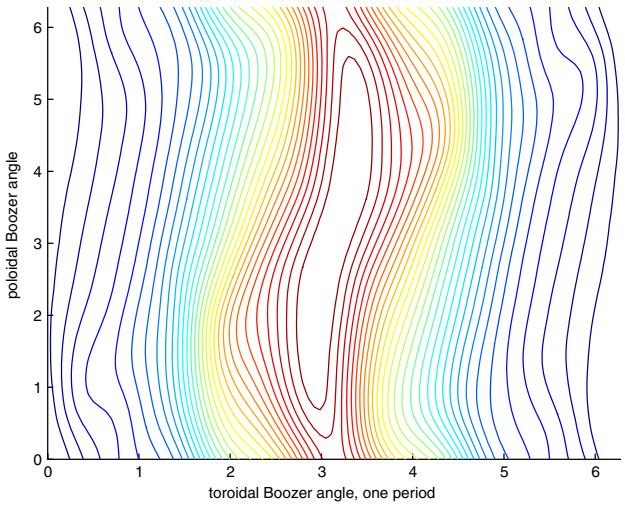

Figure 3. The contours of B on the magnetic surface (at half of the minor plasma radius). It is seen that a small residual local maximum of B still exists.

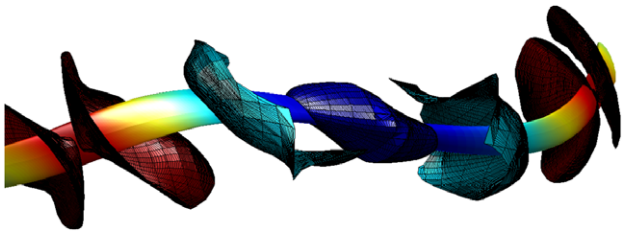

Figure 4. Near-axis magnetic surface and contours of B, six open ones and one topologically spherical one which encloses the minimum of B; the colour coding is similar to that in figures 1 and 3.

Major properties that are not targeted directly are the collisionless α-particle confinement (as opposed to earlier optimizations [4]) and the MHD stability with respect to nonlocal ballooning-type [11] as well as free-boundary modes [12], whose growth rates are given, too. Also, a vacuum field magnetic well is not targeted.

3. Results

Here, results of the integrated optimization are presented in detail. In figures 2–4 the geometrical outlook of the configuration together with its structure of the magnetic field strength is shown. As seen in figure 2, the geometry, broadly

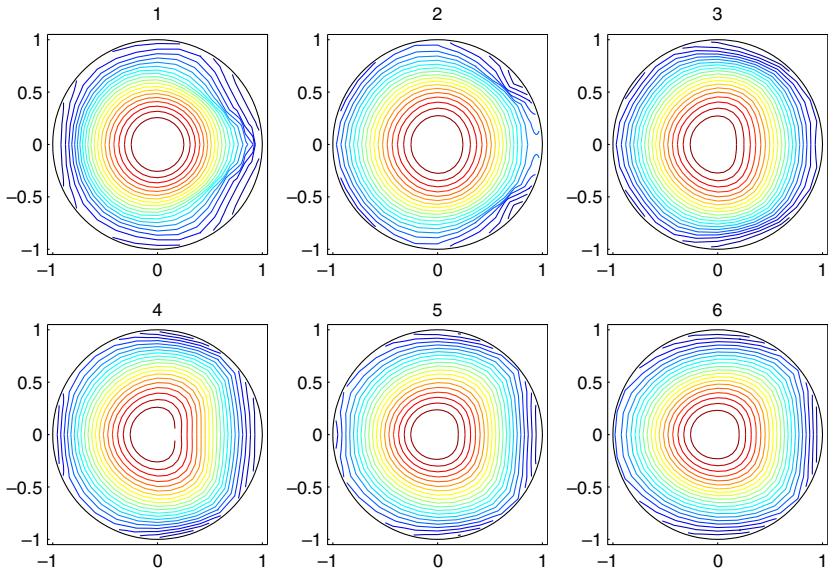

Figure 5. $\mathcal{J}$ contours for increasing values of B_{ref} in polar-coordinate representation $\sqrt{s}, \theta$ with s the flux label. Labels $i = 1, \ldots, 6$: $B_{\mathrm{ref}} = B_{\mathrm{min}} + i\,\Delta B/7$; $\Delta B = B_{\mathrm{max}} - B_{\mathrm{min}}$. The red colour corresponds to maximal value of $\mathcal{J}$ showing the max-$\mathcal{J}$ property of this configuration. The $\Delta\mathcal{J}/\mathcal{J}$ values change from ≈0.05 for the most deeply trapped to ≈0.01 for the most shallowly trapped particles.

viewed, is W7-X-like: characterized in terms of toroidal and helical plasma-column curvatures; in one-half of the periods the toroidal curvature adds to the helical curvature and here a crescent-shaped flux surface occurs whereas in the other half of the periods the toroidal curvature diminishes the helical curvature and here a triangle-shaped cross section occurs. Up to now, MHD-stable stellarators of the qh, qa and qi types all exhibit these features. The special feature associated with the poloidal closure of B toroidally everywhere is the region near the crescent-shaped cross section. As a result of the integrated optimization a toroidally rather narrow nearly straight plasma section is established there so that the maximal strength of B is not restricted to the inner side of the crescent cross section as in W7-X but occurs throughout it. In figure 3 it is seen that this situation is not established perfectly within the integrated optimization but sufficiently in order to dominate the collisionless fast-particle confinement as seen below. In figure 4, one period of the plasma core centred around the triangular cross section is shown and, in relation to it, surfaces of constant B. Under the influence of the finite plasma β ($\langle\beta\rangle = 0.088$) a true minimum of B exists at the triangular cross section, so that a closed surface of B exists there. With increasing toroidal distance from this minimum the surfaces become open but still concave as seen by the reflected particles oscillating between them. This feature causes the maximum-$\mathcal{J}$ property shown in figure 5. This maximum becomes more gentle with increasing reflection value of B. At the boundary between reflected and passing particles the integration length for the second adiabatic invariant becomes the length of the field lines within one period which, for ideal quasi-isodynamicity, is a constant on flux surfaces. This length was not one of the target parameters of the integrated optimization but turns out to be essentially flat across the plasma cross section so that peripheral field lines are not significantly longer than the magnetic axis. Obviously the alignment of the contours of $\mathcal{J}$ with the magnetic surfaces is excellent as considered on the scale of the plasma radius. The

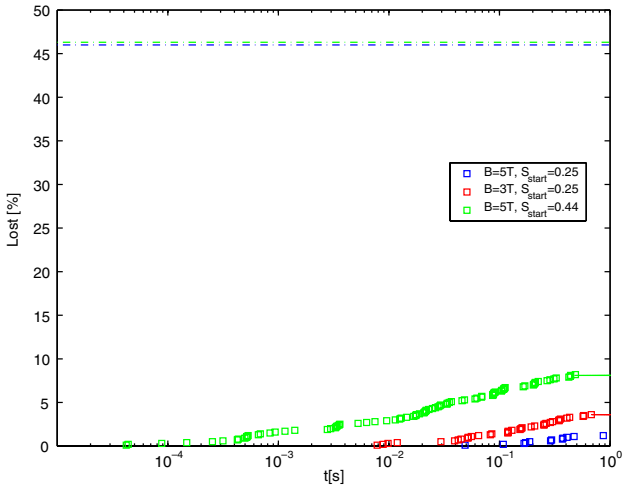

Figure 6. Loss histories of 1000 α-particles started at half and $\frac{2}{3}$ of the plasma radius and randomly distributed in the angular variables and the pitch angle. Normalization: plasma volume 10^3 m^3, magnetic fields 5 T (blue and green) and 3 T (red). Each symbol marks the loss of one particle. The lines at about 46% indicate the fractions of reflected particles.

energetic-particle confinement associated with this structure of $\mathcal{J}$ contours was checked independently and found to be excellent, see figure 6.

On the scale of deviations of collisionless electrons from flux surfaces, however, these deviations are substantial so that the $\mathcal{J}$-contour optimization is in practice not sufficient to guarantee a sufficiently low level of $1/\nu$ transport of the electrons in the lmfp regime. Therefore, the equivalent ripple has been used as an additional target parameter in the integrated optimization. Figure 7 shows the result which is similar to the one obtained for W7-X [5, 6].

The last neoclassical property to be described is the bootstrap current behaviour. As shown in the appendix the

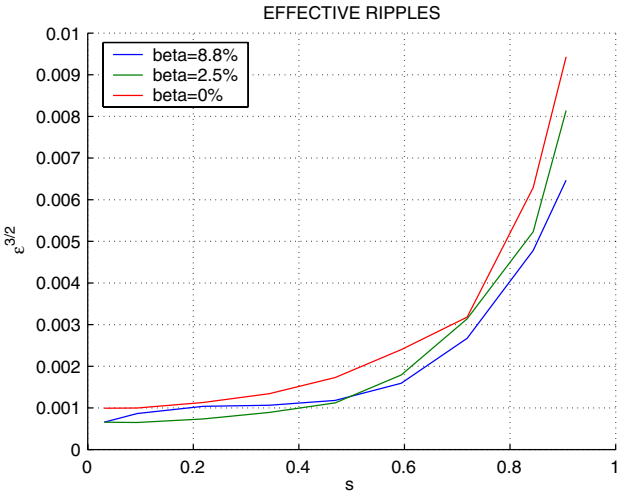

Figure 7. Equivalent ripple to the $\frac{3}{2}$ power as a function of the normalized toroidal flux for different values of β. Values for W7-X [5] are 0.0012 at $s = 0.1$, 0.001 at 0.5, 0.0015 at 1.

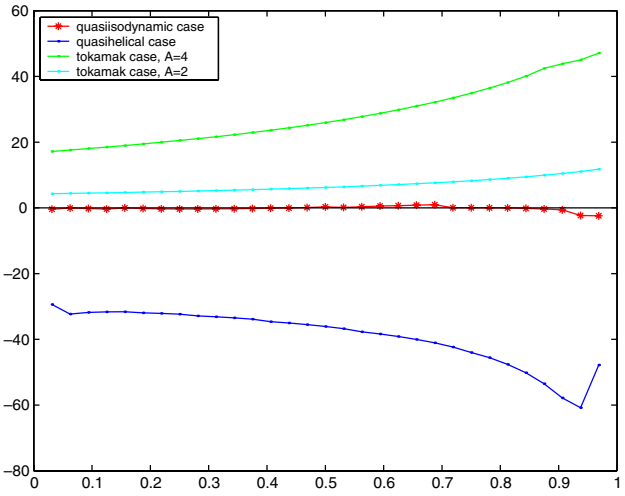

Figure 8. The structural factor of the bootstrap current as a function of the normalized toroidal flux in comparison with two tokamak (aspect ratio 2 (lower positive bs factor) and 4 (higher positive bs factor) and a quasi-helically symmetric [15] configurations approximately equivalent in aspect ratio and rotational transform. The bs factor used here contains the square of the aspect ratio in order to be normalized in such a way that it indicates $\Delta\iota/\iota$, the relative change in the rotational transform due to the bs current. The two tokamak cases are shown to demonstrate this aspect ratio dependence.

structural factor of the bootstrap current in the lmfp regime vanishes for ideal quasi-isodynamicity of configurations with poloidally closed contours of B. In accordance with this concurrence the annihilation of this structural factor is targeted in the integrated optimization and very well achieved. Figure 8 shows this result in comparison with quasi-helically symmetric and axisymmetric equivalent configurations. Also, the current–density lines which are not targeted in the integrated optimization, reflect their associated behaviour, i.e. approximately closed in one period, see figure 9.

Summarizing these findings one may conclude that the neoclassical properties of the configuration obtained are

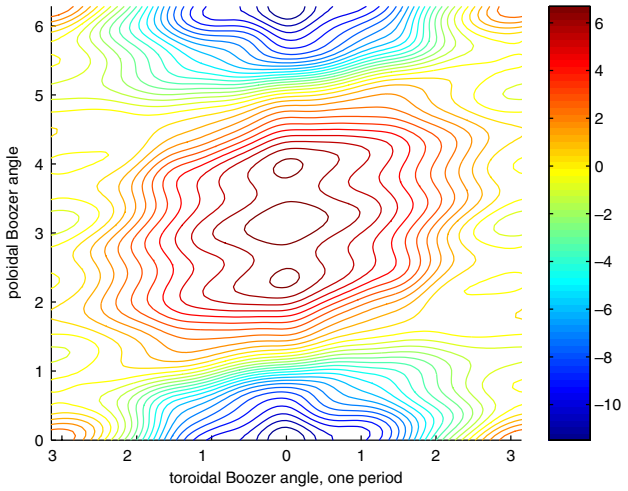

Figure 9. Contours of $j_\parallel/B$ at half the plasma radius.

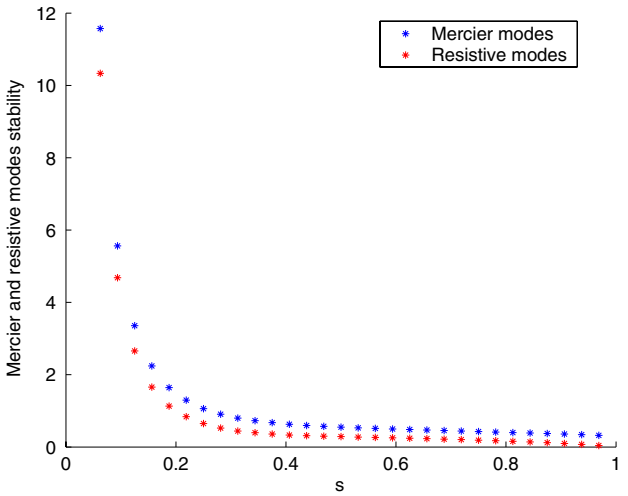

Figure 10. The Mercier- and resistive-interchange stability criteria at $\langle\beta\rangle = 0.088$.

sufficiently benign. These properties hold simultaneously with the MHD properties discussed below.

As basic requirements for low-shear stellarators a rotational transform increasing to the outside and falling into a window free of low-order rational values is considered as a target for equilibria without net toroidal current; this window is chosen to be $\frac{6}{7} < \iota < \frac{6}{6}$. Stability of Mercier- as well as resistive-interchange-mode criteria is maintained, see figure 10, for an equilibrium with $\langle\beta\rangle = 0.088$ in order to avoid low-node-number internal and external ideal MHD modes.

The behaviour with respect to local ballooning modes is characterized as follows. While they are unstable at $\langle\beta\rangle = 0.088$, see figure 11 (top), they become stable at $\langle\beta\rangle = 0.065$. With a view to the stability of nonlocal modes, see below, they must be small-scale modes in the range between 0.065 and 0.085.

With respect to non-local MHD modes, the stability properties are characterized by two types of stability calculations with CAS3D (see, e.g. [11]). First, a stability boundary, $\langle\beta\rangle = 0.085$, is obtained with nonlocal,

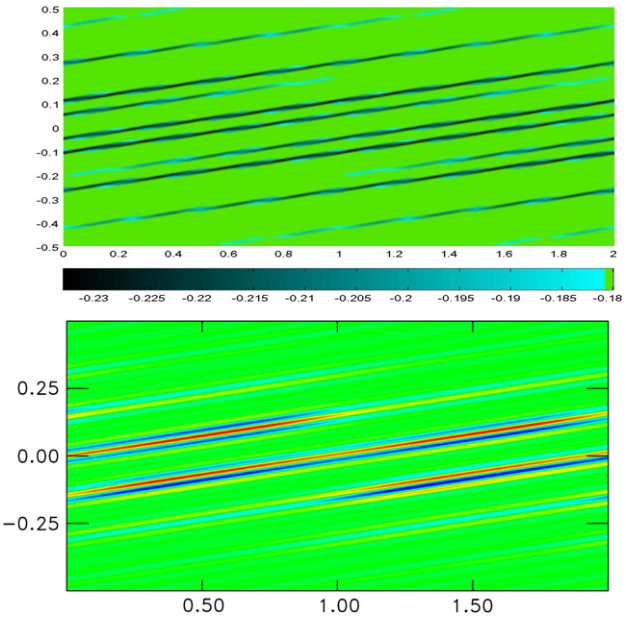

Figure 11. Most unstable (blue) regions on a magnetic surface as obtained from the local-ballooning analysis (top); normal displacement of a nonlocal ballooning mode on the same magnetic surface (bottom). Shown are two out of six periods (vertical: $-0.5 < \theta < 0.5$, horizontal: $0 < \phi < 2$, the latter value corresponding to two periods). In detail (bottom): contours for the most unstable medium-node-number perturbation at $\langle\beta\rangle = 0.088$ on the magnetic surface enclosing half of the normalized toroidal flux, $s = 0.5$. Dark blue (red) is for strong inward (outward) normal displacement which occurs in a band on the outside of the torus around $\theta = 0$. Computation parameters: 101 radial points, 280 normal displacement harmonics, field-perturbation normalization, vanishing adiabatic index $\gamma = 0$, $N = 1$ mode family, phase-factor transform [16] with $M = 20$, $N = -19$.

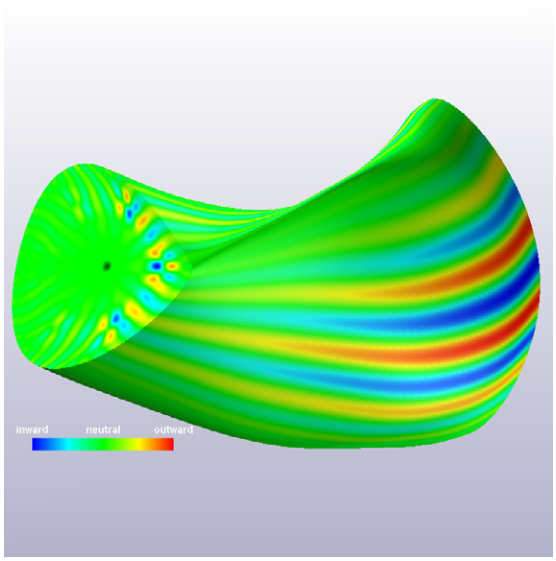

Figure 12. Normal displacement contours for the most unstable medium-node-number free-boundary perturbation at $\langle\beta\rangle = 0.1$. One-half of six field periods of the plasma column is shown with the tip of the triangular cross-section pointing to the outside of the torus. Dark blue (red) is for strong inward (outward) normal displacement. Computation parameters: 101 radial points, 279 normal displacement harmonics, 279 (721) η (μ) harmonics describing the in-surface displacement, kinetic-energy normalization, adiabatic index $\gamma = 5/3$, $N = 1$ mode family, infinite vacuum region.

however medium-scale modes by employing an eigenmode normalization eliminating the shear-Alfvén continuum (cf [13]). The mode structure of this mode is seen in figure 11 (bottom). The comparison of the structures, local ballooning versus amplitude of nonlocal mode, shows their close correspondence. Second, the growth times (e-folding times) of medium-scale free-boundary modes at $\langle\beta\rangle = 0.09$ and $\langle\beta\rangle = 0.10$ are obtained with the kinetic energy as physically appropriate normalization; they are given by $\tau_e = \sqrt{\mu_o \rho_o(0)/|\lambda_{MHD}|}$ with μ_o the permeability of free space, $\rho_o(0)$ the mass density at the magnetic axis and λ_{MHD} the eigenvalue in MHD-convenient normalization (square of perturbation field divided by perturbation) $(T/m)^2$. Thus, $\tau_e = B/(v_A\sqrt{|\lambda_{MHD}|}) = [B/(L_{curv}\sqrt{|\lambda_{MHD}|})]\tau_A$ with the Alfvén speed at the magnetic axis taken with the average B there and an Alfvén time defined by $\tau_A = L_{curv}/v_A$ with L_{curv} the connection length between favourable- and unfavourable-curvature regions which, in qi stellarators, is approximately half the period length. For W7-X-typical high-β parameters (deuterons, $n(0) = 3 \cdot 10^{20}$, $B_o = 1$, $L_{curv} \approx 3.5$ in SI units), $\tau_e \approx 26\,\mu s \approx 7\tau_A$ is found at $\langle\beta\rangle = 0.10$ and about $20\tau_A$ at $\langle\beta\rangle = 0.09$. Figure 12 shows the structure of the mode at $\langle\beta\rangle = 0.10$ revealing that the ballooning property is dominant.

Finally, figure 13 shows the geometry of the configuration obtained by way of its characteristic cross-sections and its rotational transform profile. Evaluated at $\beta = 0$, this plasma shape exhibits a small magnetic well, 0.7% (by comparison, the well in the configuration optimized for W7-X: 1%). Mercier and resistive-interchange stability holds for all β values below the one used for the optimization and the ballooning stability limit is improved [11] which indicates that the configuration found here exhibits locally less unfavourable curvatures.

4. Conclusion

With the advent of qh, qa, qi configurations it may seem that a general aspect of stellarator configurational space has been explored because all three possible directions of reflected-particle drifts—helical, axial and poloidal—are realized. Nevertheless, details of the structural properties of the stellarator configurational space remain to be explored. In this case study it has been shown that a specific combination of physical properties appears possible: the simultaneous realization of a high-β MHD stable plasma with low neoclassical transport, approximately vanishing bs current in the lmfp regime and excellent α-particle confinement.

Appendix

Consider a net toroidal-current (J_t) free MHD equilibrium with poloidally closed contours of the field strength B and a single minimum and a single maximum of B per period. It seems that such an equilibrium is most intuitively described by the non-periodic invariant coordinate system F_t, θ_0, B with F_t the toroidal flux labelling the magnetic surfaces and θ_0 labelling the field lines. Then

$$\vec{B} = \nabla F_t \times \nabla\theta_0.$$

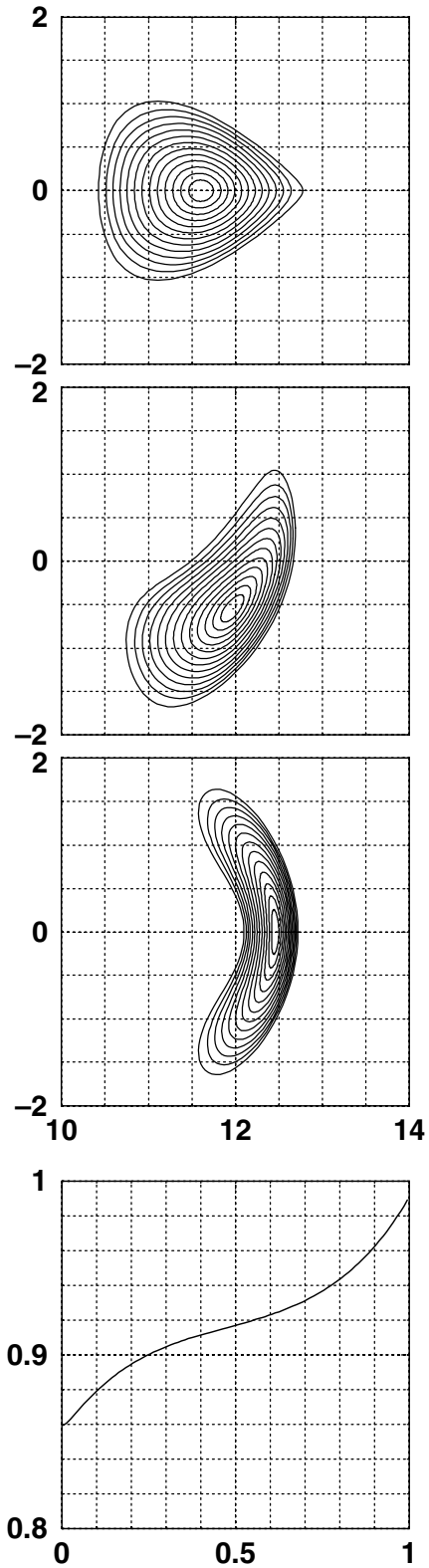

Figure 13. Flux surface cross sections at the beginning of, quarter of and half a period in the three upper panels and the profile of the rotational transform as a function of normalized toroidal flux in the lowest panel. The size normalization used is a small plasma radius of about 1, so that the axes R and z are given in this normalization.

The increment in θ_0 in one period comparing two equivalent space points is $\Delta\theta_0 = \iota_{\text{period}}$. With $\mathcal{J}$ the second adiabatic invariant and the assumption

$$\mathcal{J} = \mathcal{J}(F_\text{t}) \qquad \text{for all reflection values } \mathrm{B_{ref}}$$

one sees from $\mathcal{J} \propto \int_0^{l^+} \sqrt{B_\text{ref} - B}\,\mathrm{d}l + \int_0^{l^-} \sqrt{B_\text{ref} - B}\,\mathrm{d}l = \int_{B_\text{min}}^{B_\text{ref}} \sqrt{B_\text{ref} - B}\,\partial_B l^+ \mathrm{d}B + \int_{B_\text{min}}^{B_\text{ref}} \sqrt{B_\text{ref} - B}\,\partial_B l^- \mathrm{d}B$ (with l^-, l^+ the lengths from B_min to B^-_ref and B^+_ref) by computing $\partial_{\theta_0}\mathcal{J}$

$$\partial_{\theta_0}(\mathrm{d}l^- + \mathrm{d}l^+) = 0. \qquad (*)$$

Hence, in particular,

$$\partial_{\theta_0}\left(\int_0^{l^+_\text{max}} B\,\mathrm{d}l + \int_0^{l^-_\text{max}} B\,\mathrm{d}l\right) = 0,$$

with $l^+_\text{max}, l^-_\text{max}$ the lengths from B_min to B^+_max and B^-_max.

In addition, because of $J_\text{t} = 0$, on each rational field line (with, e.g. n toroidal turns before closure on itself)

$$nN_\text{p}\int_{B^-_\text{max}}^{B^+_\text{max}} B\,\mathrm{d}l = nN_\text{p}J_\text{p},$$

with N_p the number of periods and J_p the poloidal current per period, so that $\int_{B^-_\text{max}}^{B^+_\text{max}} B\,\mathrm{d}l = J_\text{p}$.

On the other hand, for $J_\text{t} = 0$, the orthogonals to the field lines in the magnetic surfaces are closed and $J_\text{p} = \int \vec{B}\cdot\vec{\mathrm{d}l}$ between any two points on the same magnetic surface on two orthogonals one period apart. Starting the integration from an intersection $\theta_{0,1}$ of an orthogonal to $\vec{B}$ with a B_max line one sees that, after one period, the corresponding orthogonal must intersect the corresponding B_max line at $\theta_{0,1} + \iota_{\text{period}}$, too. Repeating this process shows a B_max line to be an orthogonal to the field lines. Finally, the increment in $j_\parallel/B$,

$$\Delta j_\parallel/B = -\mathrm{d}p/\mathrm{d}F_\text{t}\,\partial_{\theta_0}\int_{B^-_\text{max}}^{B^+_\text{max}} \frac{\mathrm{d}l}{B},$$

vanishes because of (*) so that the current density lines are closed within one period between the B_max lines.

The bs current in the lmfp regime vanishes if two integrals with the same structure as above, i.e. functions of B (most compactly given, e.g. in [14]) integrated between B_max contours one period apart, vanish.

Similarly, because of

$$\frac{\mathrm{d}F_\text{t}}{\mathrm{d}t} = -\frac{1}{qB^2}\left(\frac{mv_\parallel^2}{B} + \mu\right)(\vec{B}\times\nabla F_\text{t})\cdot\nabla B$$

the increment per period of F_t for passing particles, ΔF_t, vanishes, too, so that the magnetic surfaces and the drift surfaces of passing particles osculate at the B_max contours.

Acknowledgments

This work was partially supported by the INTAS Grant No 99-00592, the Russian-Germany agreement WTZ-V RUS-563-98, the Russian Federal Program on support of leading scientific schools, Grant No 00-15-96526, the Russian Fund for Basic Research, Grant No 00-02-17105, and the Fonds National Suisse de la Recherche Scientifique and Euratom.

References

[1] Lotz W., Merkel P., Nührenberg J. and Strumberger E. 1992 *Plasma Phys. Control. Fusion* **34** 1037

[2] Cooper W.A. *et al* 2002 *Proc. 19th Int. Conf. on Fusion Energy 2002 (Lyon, 2002)* (Vienna: IAEA) CD-ROM file IC/P-06 and http://www.iaea.org/programmes/ripc/physics/fec2002/html/fec2002.htm

[3] Mikhailov M.I. *et al* 2002 *Nucl. Fusion* **42** L23

[4] Gori S., Lotz W. and Nührenberg J. 1996 *Theory of Fusion Plasmas (International School of Plasma Physics)* (Bologna: SIF) p 335

[5] Nemov V.V. *et al* 2003 *Plasma Phys. Control. Fusion* **45** 43

[6] Nemov V.V. *et al* 2004 *Plasma Phys. Control. Fusion* **46** 179

[7] Subbotin A.A. *et al* 2003 *30th EPS Conf. on Controlled Fusion Plasma Physics (St Petersburg, Russia, 7–11 July 2003)* vol 27A (ECA) P-4.16

[8] Nührenberg J. and Zille R. 1988 *Theory of Fusion Plasmas (Varenna, 1987)* (Bologna: Editrice Compositori) p 3

[9] Subbotin A.A. *et al* 2003 Modification of the stellarator optimization procedure by including the effective ripples and bootstrap current structural factor calculations *IAEA Technical Meeting on Innovative Concepts and Theory of Stellarators (Greifswald, 29 September–1 October 2003)* http://www.ipp.mpg.de/eng/for/bereiche/stellarator/TCM2003/IAEA2003pdf/subbotin.pdf

[10] Hirshman S.P. and Betancourt O. 1991 *J. Comput. Phys.* **96** 99

[11] Nührenberg C. 2003 *30th EPS Conf. on Controlled Fusion and Plasma Physics (St Petersburg, Russia, 2003)* vol 27A (ECA) P-1.16

[12] Nührenberg C. 2005 *32nd EPS Conf. on Controlled Fusion and Plasma Physics (Tarragona, 2005)* vol 29C (ECA) P4.057

[13] Nührenberg C. and Boozer A.H. 2003 *Phys. Plasmas* **10** 2840

[14] Johnson J.L. *et al* 1995 *Phys. Plasmas* **6** 2513

[15] Nührenberg J. and Zille R. 1988 *Phys. Lett.* A **129** 113

[16] Schwab C. 1993 *Phys. Fluids* B **5** 3195